A high-order multiscale finite-element method for time-domain elastic wave modeling in strongly heterogeneous media

Fu, Shubin
Gao, Kai
Chung,Eric

To be published in: Journal of Applied Geophysics

DOI to publisher's version: 10.1016/j.jappgeo.2019.103852

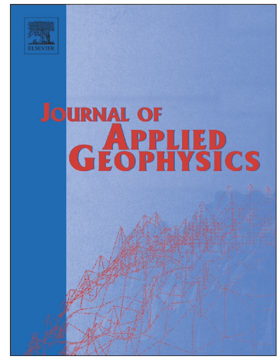

A high-order multiscale finite-element method for time-domain elastic wave modeling in strongly heterogeneous media

Shubin Fu, Kai Gao, Eric T. Chung

PII: S0926-9851(19)30153-3

DOI: https://doi.org/10.1016/j.jappgeo.2019.103852

Reference: APPGEO 103852

To appear in: *Journal of Applied Geophysics*

Received date: 17 February 2019

Revised date: 13 August 2019

Accepted date: 10 September 2019

Please cite this article as: S. Fu, K. Gao and E.T. Chung, A high-order multiscale finite-element method for time-domain elastic wave modeling in strongly heterogeneous media, *Journal of Applied Geophysics*(2018), https://doi.org/10.1016/j.jappgeo.2019.103852

A high-order multiscale finite-element method for time-domain elastic wave modeling in strongly heterogeneous media

Shubin Fu[1,*] shubinfu89@gmail.com, Kai Gao[2] and Eric T. Chung[1]
[1]Department of Mathematics, The Chinese University of Hong Kong, Hong Kong SAR
[2]Geophysics Group, Los Alamos National Laboratory, NM 87545, USA
[*]Corresponding author.

Abstract

Efficient and accurate numerical methods for elastic wave modeling in complex media have many important applications. However, it is fairly challenging to model elastic wave propagation in strongly heterogeneous media with high computational efficiency and high-order accuracy simultaneously. We develop a novel high-order multiscale finite-element method to model elastic wave propagation in strongly heterogeneous media in the time domain. The most important feature of our method is a generalization of standard multiscale finite element method by using high-order multiscale finite-element basis functions to capture the fine-scale heterogeneities on the coarse mesh, in contrast to conventional finite-element basis functions that are merely determined by the order of polynomials. These multiscale basis functions leads to a system matrix with significantly reduced dimension, thus enable us to solve the elastic wave equation on the coarse mesh with high-order accuracy and very low computational time cost. We use 2D and 3D numerical examples to demonstrate the superior efficiency and accuracy of our new modeling method compared with the conventional spectral-element method.

1 Introduction

Accurate and efficient elastic wave modeling in complex, heterogeneous media is an important task in such as seismological and civil engineering applications. The challenge of elastic wave modeling mainly comes from the fact that, for highly heterogeneous media, or when a high-frequency source wavelet is required, the mesh discretization has to be sufficiently fine to capture medium heterogeneities and wavefield variations. For large-scale, realistic applications that involves tens of millions or even billions of grids or elements, the computational costs associated with the elastic wave modeling on such fine meshes can become prohibitively high in some 3D or even 2D scenarios.

Numerical methods for elastic wave modeling include such as finite-difference methods [e.g., 53, 34, 35, 39], finite-element methods [e.g., 31, 54, 6, 56, 10, 37], pseudo-spectral methods [e.g., 18], etc. The elastic wave equation can be solved either in the time domain [e.g., 53, 31, 54, 33] or the frequency domain [e.g., 51, 48, 14, 1].

For frequency-domain elastic wave modeling, the computation costs comes from solving a large, sparse, ill-posed linear system. It is usually necessary to adopt specialized techniques to solve this linear system [e.g., 50, 15, 43, 26, 41, 16, 42]. Generally, obtaining accurate solutions to the elastic wave Helmholtz equation requires non-trivial coding and computational efforts. There exist fairly a large amount of adaptive methods, including finite-difference methods [47, 52], spectral-element method [46], finite-element and enriched finite-element methods [49], plane-wave and generalized plane-wave methods [3, 27, 28], and polynomial Galerkin methods with hp refinement [38, 57], etc, to solve the frequency-domain elastic wave equation.

On the other hand, time-domain elastic wave modeling is more popular in most applications because time-domain solvers are usually simpler to implement on parallel computing architectures and have higher computational efficiency compared with the frequency-domain approach. Relevant studies consist of a large repository that we have no intention to completely review. Finite-difference methods for time-domain elastic wave modeling employ various kinds of discretization schemes [e.g., 53, 34, 44, 55, 40, 35, 36, 24]. The direct discretization of the elastic wave equation by finite-difference methods leads to computationally efficient algorithms. However, finite-difference methods are mostly limited to structured mesh applications. For elastic wave modeling on unstructured meshes, it is necessary to apply finite-element based approaches, of which the spectral-element method [e.g., 32, 31, 9, 33] seems to be the most efficient because of the resulting mass matrix is strictly diagonal in spectral-element methods. This is an extremely important feature for time-domain applications. In [29], the authors developed an arbitrary high-order discontinuous Galerkin method for elastic wave propagation using both spatial and temporal high-order schemes using the arbitrary high-order derivatives for flux calculation. Authors in [54] developed a high-order accurate discontinuous Galerkin approach for wavefield modeling in coupled acoustic-elastic media by deriving the explicit expressions for the upwind numerical flux. The anisotropic scenario of their method is given by [56]. The interior penalty discontinuous Galerkin method for elastic wave propagation was explored in [11] , which can be used to simulate elastic wave propagation in fractured media. There are also other approaches that exploit the staggered finite element to improve the accuracy of elastic wave modeling [7, 8].

Our method for time-domain elastic wave modeling originates from the multiscale finite-element methods (MsFEM) and generalized multiscale finite-element methods (GMsFEM), which attempts to reduce the computational time cost associated with solving a partial differential system using multiscale basis functions. Originally developed for solving elliptic-type partial differential equations [12, 30, 13, 45], MsFEM and GMsFEM have been successfully developed and extended for solving wave propagation problems in the time or the frequency domain [e.g., 4, 19, 25, 5, 21, 20, 23]. In MsFEM or GMsFEM, the wave equation is solved on the coarse mesh instead of the fine mesh, and the fine-level medium properties and coarse-level wavefield solutions are connected by medium-dependent multiscale basis functions. These multiscale basis functions are solved from local static problems that incorporate local medium information. Using medium-dependent multiscale basis functions is the most important feature of the multiscale finite-element method compared with the conventional finite-element or spectral-element method (SEM) [e.g., 31, 33].

Studies [22, 23] show that using high-order multiscale basis functions leads to higher-order accurate wavefield solution for multiscale finite-element methods. In the first-order approaches [e.g., 19, 5, 21], the multiscale basis functions are constructed based on solving local spectral problems in coarse blocks. It is then necessary to select the first several eigenvectors corresponding to the smallest eigenvalues to construct the multiscale basis functions. The number of eigenvectors selected for this construction determines the accuracy of the final solution. In this study, we develop a different and novel approach to constructing high-order multiscale basis functions using local linear problems instead of local spectral problems. We use two different types of local problems to solve for boundary and interior basis functions, and construct the final multiscale basis functions by linearly combining the resulting local problem solutions. The linear combination coefficients are determined based on the cardinal property of these local linear problem solutions in space. With these multiscale basis functions, the dimensions of the global systems are significantly reduced dimensions compared with those assembled on the fine mesh. The computation time cost associated with solving this linear system is therefore significantly smaller than that using conventional methods. We call our method the high-order multiscale finite-element method (HMsFEM). We use a 2D numerical example and a 3D numerical example to demonstrate the efficiency and the accuracy of our HMsFEM, and show that our HMsFEM is evidently more efficient compared with the conventional spectral-element method (SEM) for modeling elastic wave propagation in strongly heterogeneous media.

Our HMsFEM can be viewed as a generalization of the original MsFEM applied to wave equation simulation problem. The most important feature of our HMsFEM is that we employ high-order basis functions in both the fine-scale level and the coarse-scale level. In the fine-scale level, we use conventional high-order Lagrange polynomial basis functions based on the high-order Gauss-Lobatto-Legendre (GLL) nodes. On the coarse-scale level, we use medium-dependent high-order multiscale basis functions that are closely related to the high-order GLL nodes of the coarse element. Such a strategy ensures that we obtain high-order accurate solution to the elastic-wave equation on the coarse mesh in strongly heterogeneous media.

Our paper is organized as follows. In the Methodology section, we describe the construction of our HMsFEM for time-domain elastic wave equation modeling, particularly the details of constructing high-order multiscale basis functions from local linear problems. We then use two numerical examples to demonstrate the efficiency and accuracy of our HMsFEM for elastic wave modeling in strongly heterogeneous media in the Numerical Results section. We draw conclusions to our method in the Conclusions section.

2 Methodology

2.1 Elastic wave equation

The time-domain elastic wave equation in general anisotropic media can be written as

$$\rho \frac{\partial^2 \mathbf{u}}{\partial t^2} - \nabla \cdot \boldsymbol{\sigma}(\mathbf{u}) = \mathbf{f}, \tag{1a}$$

$$\boldsymbol{\sigma}(\mathbf{u}) = \mathbf{c} : \boldsymbol{\varepsilon}(\mathbf{u}), \tag{1b}$$

$$\boldsymbol{\varepsilon}(\mathbf{u}) = \frac{1}{2}\left[\nabla \mathbf{u} + (\nabla \mathbf{u})^{\mathrm{T}}\right] \tag{1c}$$

where the particle displacement wavefield $\mathbf{u} = \mathbf{u}(\mathbf{x},t) = (u_1, u_2, u_3)$, $\boldsymbol{\sigma}(\mathbf{u}) = \boldsymbol{\sigma}(\mathbf{x},t) = \sigma_{ij}$ is the stress wavefield, $\boldsymbol{\varepsilon}(\mathbf{u}) = \boldsymbol{\varepsilon}(\mathbf{x},t) = \varepsilon_{ij}$ is the strain wavefield, $\mathbf{c} = \mathbf{c}(\mathbf{x}) = c_{ijkl}$ with $i, j, k, l = 1,3$ is the rank-4 elasticity tensor, $\rho = \rho(\mathbf{x})$ is the density, and $\mathbf{f} = \mathbf{f}(\mathbf{x},t) = (f_1, f_2, f_3)$ is the external force vector. Without loss of generality, we use a point force $\mathbf{f}(\mathbf{x},t)\delta(\mathbf{x}_s)$ in our theory development and the numerical examples. In addition, we use the Voigt notation [e.g., 2] to simplify the expression of the elasticity tensor c_{ijkl} for practical computation. After the conversion, the elasticity can be expressed in a rank-2 3×3 tensor, i.e., a 3×3 symmetric matrix in the 2D case and a 6×6 symmetric matrix in the 3D case.

We define the multiscale basis function space be the set of high-order multiscale basis functions for the coarse element K_i as

$$P_H = \bigoplus_{K_H}\{\Xi_i\}, \tag{2}$$

where $\{\Xi_i\}$ is the set of high-order multiscale basis functions corresponding to K_i, and K_H is the coarse mesh. We show the methodology of constructing $\{\Xi_i\}$ in the next section.

Solving eq. (1) is equivalent to seeking $\mathbf{u}_H \in P_H \times \mathbb{R}^1$ such that

$$\int_\Omega \rho \frac{\partial^2 \mathbf{u}_H}{\partial t^2} \cdot \mathbf{w}_H d\mathbf{x} + \int_\Omega \boldsymbol{\sigma}(\mathbf{u}_H) : \boldsymbol{\varepsilon}(\mathbf{w}_H) d\mathbf{x} = \int_\Omega \mathbf{f}_H \cdot \mathbf{w}_H d\mathbf{x} \tag{3}$$

for any test function $\mathbf{w}_H \in P_H$, where Ω is the specified computational domain. In addition, we assume $\boldsymbol{\sigma}(\mathbf{u}_H)\cdot\mathbf{n} = 0$ where $\mathbf{n}$ is the outward pointed normal of $\partial\Omega$.

The mesh discretization for our HMsFEM is different from that in the conventional finite-element methods. Specifically, the mesh in our HMsFEM is a two-level composite mesh composed of a coarse mesh K_H overlaying a fine mesh K_h, as shown in Fig. 1. Each of the coarse elements consist of multiple finer elements. We employ a high-order spectral-element type fine mesh to achieve high-order accuracy for elastic wave modeling in complex media, which indicates that in each of fine elements, there are high-order GLL nodes that represent the finer element's degrees of freedom [e.g., 31].

Figure 1: A two-level composite mesh adopted in our HMsFEM. The blue thick lines indicate the coarse mesh, while the black thin lines indicate the fine mesh. In our numerical tests, we use a simple structured mesh, which is a simplified version of the mesh shown in this Figure.

2.2 High-order multiscale basis functions

Employing high-order multiscale basis functions for dimension reduction is the most important feature of our HMsFEM for time-domain elastic wave modeling. In first-order MsFEMs [e.g., 21], we construct first-order multiscale basis functions using local spectral problems to capture local medium properties. In HMsFEM, the construction of the high-order, medium-dependent multiscale basis functions is different from that for the first-order MsFEMs. We show the methodology of constructing high-order multiscale basis functions as below.

In our high-order MsFEM, we construct the multiscale basis functions from two different types of local bases, namely the boundary high-order multiscale basis functions and the interior high-order multiscale basis functions, both solved from local, static elasticity equations.

To construct the boundary high-order multiscale basis functions, we solve the following local static elasticity problem in each of the coarse elements in the computational domain:

$$-\nabla \cdot \boldsymbol{\sigma}(\boldsymbol{\Psi}_i) = 0, \tag{4}$$

where $i = 1, 2, \cdots, N_1$ is the index of the boundary nodes of a coarse element K, $N_1 = 4m$ is the total number of boundary nodes of a coarse element K (indicated by the black circles in Fig. 2), and m is the order of the Lagrange interpolation polynomial [e.g., 31, 17]. For simplicity, we assume m is same along different spatial axes, which can be different along different axes for better flexibility.

The multiscale basis functions are constructed corresponding to each of the displacement wavefield components. Specifically, we set the local problem (4) with the following boundary conditions to obtain the boundary bases corresponding to the first displacement component:

$$\Psi_{1,i} = \xi_i, \qquad \Psi_{2,i} = 0, \qquad \Psi_{3,i} = 0, \tag{5}$$

where ξ_i is the Legendre shape function corresponding to the i-th GLL node that lies on the boundary of the coarse element ∂K, and the subscripts 1, 2 and 3 of Ψ indicate the first, the second and the third displacement components, respectively. To solve for the basis functions corresponding to the second and the third displacement components, we set the boundary conditions to be

$$\Psi_{1,i} = 0, \qquad \Psi_{2,i} = \xi_i, \qquad \Psi_{3,i} = 0, \tag{6}$$

$$\Psi_{1,i} = 0, \qquad \Psi_{2,i} = 0, \qquad \Psi_{3,i} = \xi_i, \tag{7}$$

respectively, and solve the local problem in eq. (4) with these boundary conditions accordingly.

To solve these local problems, we employ the high-order spectral-element method to achieve high-order accuracy. To save computational costs, we solve the three local problems corresponding to the three displacement components simultaneously. We denote the basis functions obtained from the first problem as $\tilde{\mathbf{\Psi}} = \{\mathbf{\Psi}^{[1]}, \mathbf{\Psi}^{[2]}, \mathbf{\Psi}^{[3]}\}$, where the superscript $[i]$ indicates the corresponding basis is solved for the i-th displacement component.

It is obvious that the boundary basis functions are naturally medium-dependent. In heterogeneous media, the boundary basis functions are different in different coarse elements. It is also clear that the total number of the boundary basis functions is $3N_1$, where N_1 is the total number of the boundary nodes of a coarse element.

We the construct the second type high-order multiscale basis function, namely the interior high-order multiscale basis functions, using a different local static elasticity problem as below:

$$-\nabla \cdot \boldsymbol{\sigma}(\mathbf{\Phi}_j) = \mathbf{Q}_j^{[1]}, \tag{8}$$

where $\mathbf{Q}_j^{[1]}$ is a vector function composed of polynomials. The subscript $j = 1, 2, \cdots, N_2$ is the index looping over all the interior GLL nodes of a coarse element (the black disks in Fig. 2), and $N_2 = (m-1)^3$ is the total number of the interior GLL nodes for a 3D coarse element.

To solve for the interior basis functions corresponding to the first displacement component, we set the right hand side of eq. (8) to be

$$\mathbf{Q}_j^{[1]} = (\zeta_j, 0, 0), \tag{9}$$

with zero Dirichlet boundary conditions, i.e.,

$$\Phi_{1,j} = \Phi_{2,j} = \Phi_{3,j} = 0 \quad \text{on} \quad \partial K. \tag{10}$$

To solve for the high-order interior multiscale basis functions corresponding to the second and the third displacement components, we set the right hand side source term to be

$$\mathbf{Q}_j^{[2]} = (0, \zeta_j, 0), \tag{11}$$

$$\mathbf{Q}_j^{[3]} = (0, 0, \zeta_j), \tag{12}$$

respectively. We denote the interior basis functions obtained from the above local as $\tilde{\mathbf{\Phi}} = \{\mathbf{\Phi}^{[1]}, \mathbf{\Phi}^{[2]}, \mathbf{\Phi}^{[3]}\}$. It is evident that the interior multiscale basis functions are also medium-dependent as the boundary basis functions, and the total number of the interior basis functions set is $3N_2$, where N_2 is the total number of interior GLL nodes of a coarse element K .

In our HMsFEM, we represent each individual displacement component by a vector multiscale basis function instead of a scalar basis. Using the solved boundary and interior basis functions, we express the vector high-order multiscale basis functions as a linear combination of all the boundary and interior basis functions:

$$\boldsymbol{\Xi}^{(l)}(\mathbf{x}) = \sum_{i=1}^{3N_1} \alpha_i^{(l)} \tilde{\boldsymbol{\Psi}}_i(\mathbf{x}) + \sum_{j=1}^{3N_2} \beta_j^{(l)} \tilde{\boldsymbol{\Phi}}_j(\mathbf{x}), \tag{13}$$

where $\alpha_i^{(l)}$ and $\beta_j^{(l)}$ are combination coefficients corresponding to the l-th basis of a coarse element.

The problem is how to compute the linear combination coefficients that are suitable for time-domain elastic wave modeling. We determined the linear combination coefficients α_i and β_j using the cardinal interpolation property of the multiscale basis functions, which reads

$$\boldsymbol{\Xi}^{(l)}(\mathbf{x}_r) = (\boldsymbol{\delta}_{lr}, 0, 0) \quad \text{or} \quad (0, \boldsymbol{\delta}_{lr}, 0) \quad \text{or} \quad (0, 0, \boldsymbol{\delta}_{lr}), \tag{14}$$

in which $\mathbf{x}_r$ represents the r-th GLL node in the coarse element. In the HMsFEM developed for acoustic wave equation modeling, a similar approach for linear combination coefficient determination is used in [23] . In the context of the conventional SEM, this property holds for the Lagrange interpolation functions [e.g., 17]. With $\mathbf{x}_h$ and $\mathbf{x}_l$ denoting different GLL nodes in a coarse element, the above property can be written as

$$\sum_{i=1}^{3N_1} \alpha_i^{(l)} \tilde{\boldsymbol{\Psi}}_i(\mathbf{x}_l) + \sum_{j=1}^{3N_2} \beta_j^{(l)} \tilde{\boldsymbol{\Phi}}_j(\mathbf{x}_l) = (1, 0, 0), \tag{15a}$$

$$\sum_{i=1}^{3N_1} \alpha_i^{(l)} \tilde{\boldsymbol{\Psi}}_i(\mathbf{x}_h) + \sum_{j=1}^{3N_2} \beta_j^{(l)} \tilde{\boldsymbol{\Phi}}_j(\mathbf{x}_h) = (0, 0, 0), \tag{15b}$$

for $h \neq l$ with $l \leq N_1 + N_2$, and

$$\sum_{i=1}^{3N_1} \alpha_i^{(l)} \tilde{\boldsymbol{\Psi}}_i(\mathbf{x}_{l'}) + \sum_{j=1}^{3N_2} \beta_j^{(l)} \tilde{\boldsymbol{\Phi}}_j(\mathbf{x}_{l'}) = (0, 1, 0), \tag{16a}$$

$$\sum_{i=1}^{3N_1} \alpha_i^{(l)} \tilde{\boldsymbol{\Psi}}_i(\mathbf{x}_h) + \sum_{j=1}^{3N_2} \beta_j^{(l)} \tilde{\boldsymbol{\Phi}}_j(\mathbf{x}_h) = (0, 0, 0), \tag{16b}$$

for $l' = l - (N_1 + N_2)$, $h \neq l'$ with $N_1 + N_2 < l <= 2(N_1 + N_2)$, and

$$\sum_{i=1}^{3N_1} \alpha_i^{(l)} \tilde{\boldsymbol{\Psi}}_i(\mathbf{x}_{l''}) + \sum_{j=1}^{3N_2} \beta_j^{(l)} \tilde{\boldsymbol{\Phi}}_j(\mathbf{x}_{l''}) = (0, 0, 1), \tag{17a}$$

$$\sum_{i=1}^{3N_1}\alpha_i^{(l)}\tilde{\mathbf{\Psi}}_i(\mathbf{x}_h)+\sum_{j=1}^{3N_2}\beta_j^{(l)}\tilde{\mathbf{\Phi}}_j(\mathbf{x}_h)=(0,0,0), \tag{17b}$$

for $l''=l-2(N_1+N_2)$, $h\neq l''$ with $2(N_1+N_2)<l<=3(N_1+N_2)$.

Written in a compact matrix form, this cardinal condition is

$$\begin{bmatrix} \tilde{\mathbf{\Psi}}_1(\mathbf{x}_1) & \cdots & \tilde{\mathbf{\Psi}}_{3N_1}(\mathbf{x}_1) & \tilde{\mathbf{\Phi}}_1(\mathbf{x}_1) & \cdots & \tilde{\mathbf{\Phi}}_{3N_2}(\mathbf{x}_1) \\ \tilde{\mathbf{\Psi}}_1(\mathbf{x}_2) & \cdots & \tilde{\mathbf{\Psi}}_{3N_1}(\mathbf{x}_2) & \tilde{\mathbf{\Phi}}_1(\mathbf{x}_2) & \cdots & \tilde{\mathbf{\Phi}}_{3N_2}(\mathbf{x}_2) \\ \vdots & \vdots & \vdots & \vdots & \vdots & \vdots \\ \tilde{\mathbf{\Psi}}_1(\mathbf{x}_M) & \cdots & \tilde{\mathbf{\Psi}}_{3N_1}(\mathbf{x}_M) & \tilde{\mathbf{\Phi}}_1(\mathbf{x}_M) & \cdots & \tilde{\mathbf{\Phi}}_{3N_2}(\mathbf{x}_M) \end{bmatrix} \begin{bmatrix} \alpha_1^{(l)} \\ \vdots \\ \alpha_{3N_1}^{(l)} \\ \beta_1^{(l)} \\ \vdots \\ \beta_{3N_2}^{(l)} \end{bmatrix} = \begin{bmatrix} 0 \\ \vdots \\ 1 \\ \vdots \\ 0 \end{bmatrix}, \tag{18}$$

where $M=3(N_1+N_2)$ is the total number of coarse-scale GLL nodes (see Fig. 2) of a coarse element times 3. By solving the linear system eq. (18) corresponding to each of these M basis functions, we obtain the coefficients $\alpha_i^{(l)}$ and $\beta_j^{(l)}$.

To accelerate the computation, we obtain the coefficients for all basis simultaneously by setting the right hand side of eq. (18) to a diagonal matrix. In the first-order GMsFEM, [21] developed a similar strategy to obtain the multiscale basis functions for elastic wave modeling.

With these linear combination coefficients α_i and β_j, we now obtain the complete high-order multiscale basis functions. These multiscale basis functions depend both on local medium properties and the order of Lagrange polynomials chosen for modeling.

2.3 Discretization and dimension reduction

We assemble the global mass and stiffness matrices $\mathbf{M}$ and $\mathbf{S}$ on the coarse mesh as

$$\tilde{\mathbf{M}}=\mathbf{R}\mathbf{M}\mathbf{R}^{\mathrm{T}}, \tag{19}$$

$$\tilde{\mathbf{S}}=\mathbf{R}\mathbf{S}\mathbf{R}^{\mathrm{T}}, \tag{20}$$

where $\mathbf{M}$ and $\mathbf{S}$ are the mass and stiffness matricies assembled on the fine mesh based on high-order SEM. The matrix $\mathbf{R}$ serves as a dimension reduction matrix, in which each row is a discrete representation of the computed high-order multiscale basis functions expressed in eq. (13).

After matrix assembly, we obtain the final semi-discrete elastic wave modeling system as

$$\tilde{\mathbf{M}}\frac{d^2\tilde{\mathbf{U}}}{dt^2}+\tilde{\mathbf{K}}\tilde{\mathbf{U}}=\tilde{\mathbf{F}}, \quad (21)$$

where the symbol $\tilde{}$ indicates the mass and stiffness matrices are assembled on the coarse mesh. We then solve the discrete system using some appropriate explicit time-stepping scheme.

To obtain the fine-scale solution to the elastic wave equation, we simply back-project the coarse-scale solution $\tilde{\mathbf{U}}$ onto the fine mesh using the dimension reduction matrix $\mathbf{R}^{\mathrm{T}}$, i.e., we obtain the fine-scale solution $\mathbf{U}=\mathbf{R}^{\mathrm{T}}\tilde{\mathbf{U}}$. The computational costs associated with this procedure is trivial compared with that associated with the elastic wave modeling time stepping.

We remark that the dimension of the mass and stiffness matrices $\tilde{\mathbf{M}}$ and $\tilde{\mathbf{S}}$ are both $\sum_i^N \alpha M_i$, where M_i is the number of high-order multiscale basis functions in the coarse element K_i, and N is the total number of coarse elements residing on the coarse mesh. It is simple to show that the dimensions of the reduced matrices are significantly smaller than that of the matrices assembled directly on the fine mesh. This dimension reduction achieved in our HMsFEM for elastic wave modeling is similar with that presented in [22] for the acoustic Helmholtz equation in strongly heterogeneous media.

Figure 2: A sketch of a 2D, fourth-order coarse element in our HMsFEM. The black disks represent the interior GLL nodes, while the black circles represent the boundary GLL nodes. Note that the numbers of GLL nodes can be different along different spatial axes to provide more flexibility.

3 Numerical Results

3.1 2D random fracture model

We perform all the computation on a workstation with Intel Xeon E5-2643 CPU and with Matlab. We first use a 2D random fracture model to demonstrate the efficiency of our HMsFEM in simulating elastic wave in strongly heterogeneous media.

The model is shown in Fig. 3. This 2D model is composed of 1,000 grids in both the depth and horizontal directions. The grids size is 5 m in both spatial directions. The model is composed of a homogeneous P-wave velocity background with a value of 3,700 m/s, and numerous randomly distributed thin fractures with a P-wave velocity value of 2,590 m/s. The S-wave velocity model is scaled from the P-wave velocity using a constant scaling factor of 0.6. We also assume the density is constant through the model for simplicity.

We place a source at the center of the model. The source is a Ricker wavelet with a center frequency of 15 Hz. We simulate the wavefield propagation for a total of 1 s. Figs. 4a and b show the u_1 and u_3 components of the elastic wavefield obtained using the conventional second-order SEM on the fine mesh, respectively. The randomly distributed fractures result in fairly complicated transmission and scattered wavefields. The CPU time to obtain this solution is approximately 960 s, along with an additional 63 s dedicated to matrix assembly. With 20 m coarse mesh (i.e., coarsen ratio $r = 4$), the conventional SEM reduces the CPU time to approximately 40 s and 130 s, respectively, using the second-order and third-order polynomial basis (Table 1). However, the relative errors are also large for these two cases, which are approximately 63 percent and 41 percent, respectively. These large errors indicate that these coarse-scale solutions obtained using the conventional SEM are mostly useless in practice. We have also obtained wavefield solutions using the conventional SEM on the 40 m coarse mesh (i.e., coarsen ratio $r = 8$). The CPU time is further reduced, yet the relative errors associated with the coarse-mesh SEM solutions are even larger.

By contrast, the coarse-scale solutions on the 20 m coarse mesh obtained using our second- and third-order HMsFEM are much more accurate than those obtained using the conventional SEM (Table 1). Specifically, Figs. 5a and b show u_1 and u_3 components of the elastic wavefield, respectively, obtained using our second-order HMsFEM, and Figs. 5c and d show the amplitude differences between the HMsFEM coarse-mesh solution and the conventional SEM fine-mesh solution, respectively. Figs. 6a and b show u_1 and u_3 components of the elastic wavefield, respectively, obtained using our third-order HMsFEM, and Figs. 6c and d show the amplitude differences between the HMsFEM coarse-mesh solution and the conventional SEM fine-mesh solution, respectively. The relative errors associated with our second-order HMsFEM solution is only 15.4 percent, while that associated with the third-order HMsFEM is only 2.2 percent. In comparison, the relative errors associated with the second- and third-order SEM solutions obtained on the coarse mesh are 62.9 percent and 40.7 percent, respectively. The CPU time associated with our second- and third-order HMsFEM are approximately 40 s and 130 s, respectively, which are almost identical with those associated with the conventional SEM. The only computational expensive part of our HMsFEM is the local problem solving (approximately 30 s and 100 s for the second and third-order cases, respectively). Nevertheless, the local problem solving is a one-time task (a.k.a. the offline stage) before the wavefield propagation (a.k.a. the online stage). For multi-shot applications, the multiscale basis functions need to be computed only once, and therefore our HMsFEM is obviously more efficient than the conventional SEM. The results of 40 m coarse mesh shown in Table 1 also demonstrate that our HMsFEM is more accurate on the coarse mesh than the conventional SEM.

Figure 3: A 2D model with randomly distributed low-velocity fractures. The P-wave velocity of the background homogeneous medium is 3700 m/s, while that of the fracture is 2590 m/s. The S-wave velocity of the model is simply set to be $V_s = V_p / \sqrt{3}$. The density is homogeneous for simplicity.

Figure 4: The reference wavefields at $t = 1$ s computed using the conventional SEM on the fine mesh. The panel in (a) is the u_1 component, while that in (b) is the u_3 component. The CPU time to obtain these fine-mesh SEM solutions is approximately 960 s.

Figure 5: The (a) u_1 and (b) u_3 components of the elastic wavefield solution obtained using our second-order HMsFEM on the coarse mesh. The differences between the coarse-mesh HMsFEM solutions and the fine-mesh SEM solutions are shown in (c) and (d) for the u_1 and u_3 components, respectively. The CPU time to obtain the coarse-mesh HMsFEM solutions is approximately 38 s.

Figure 6: The (a) u_1 and (b) u_3 components of the elastic wavefield solution obtained using our third-order HMsFEM on the coarse mesh. The differences between the coarse-mesh HMsFEM solutions and the fine-mesh SEM solutions are shown in (c) and (d) for the u_1 and u_3 components, respectively. The CPU time to obtain the coarse-mesh HMsFEM solutions is approximately 130 s.

Method	m	N	r	T_{offline} (s)	T_{online} (s)	ε
SEM	2	800	1	62.7	960.5	/
SEM	1	800	1	42.2	150.6	0.353
SEM	2	200	4	11.0	39.7	0.629
SEM	3	200	4	25.5	129.8	0.407
HMsFEM	2	200	4	30.3	38.4	0.154
HMsFEM	3	200	4	98.5	129.1	0.022
SEM	3	100	8	22.4	32.4	0.789
SEM	4	100	8	58.4	74.1	0.655
HMsFEM	3	100	8	133.6	32.1	0.136
HMsFEM	4	100	8	440.0	73.8	0.050

Table 1: Parameter settings, computational time costs and relative errors of the simulation results for the 2D random fracture model. The results are obtained using the conventional SEM and our HMsFEM. The parameter m is the order of fine element (for SEM) or the coarse element (for HMsFEM), N is the number of fine elements along each spatial axis, r is the coarsening ratio between the coarse element and the fine element, T_{offline} is the CPU time consumption of the offline stage measured in second, T_{online} is the CPU time consumption of the online stage measured in second, ε is the relative error defined in as $\varepsilon = \| \mathbf{u} - \mathbf{u}_0 \|_2 / \| \mathbf{u}_0 \|_2$ with $\mathbf{u}$ being the coarse-scale solution computed using either the conventional SEM or our HMsFEM. For the conventional SEM, T_{offline} is the CPU time for matrix assembly, while for our HMsFEM, T_{offline} is the CPU time for solving the local problems and matrix assembly.

3.2 3D random fracture model

We further verify the superior accuracy and efficiency of our HMsFEM over the conventional SEM using a 3D random fracture model shown in Fig. 7.

Figure 7: A 3D model with randomly distributed low-velocity disk-shaped fractures. The P-wave velocity of the background homogeneous medium is 3,700 m/s, while that of the fracture is 2,590 m/s. The S-wave velocity of the model is simply set to be $V_s = V_p / \sqrt{3}$. The density is set to be homogeneous for simplicity.

The 3D model consists of $101\times101\times101$ grids, with a grid size of 5 m in all the three spatial directions. The P- and S-wave velocity settings of the background medium and the fractures are similar with those for the aforementioned 2D random fracture model.

We place a source at the center of the model, which is a Ricker wavelet with a center frequency of 10 Hz. We simulate the wavefield propagation for a total duration of 1 s. Figs. 4a, b and c show the u_1, u_2 and u_3 components of the elastic wavefield obtained using the conventional second-order SEM on the fine mesh, respectively. The computational time to obtain the fine-mesh SEM solution is approximately 3,022 s, with an additional 781 s for the matrix assembly. On the 25 m coarse mesh (i.e., coarsen ratio $r=5$), the conventional SEM reduces the CPU time to approximately 55 s and 365 s, respectively, using the second-order and third-order polynomial basis (Table 2). The relative errors are approximately 32 percent and 26 percent, respectively.

Figs. 9a and b show u_1, u_2 and u_3 components of the elastic wavefield, respectively, obtained using our second-order HMsFEM, and Figs. 9c, d and e show the wavefield amplitude differences between the HMsFEM coarse-mesh solution and the conventional SEM fine-mesh solution, respectively. Figs. 10a, b and c show u_1, u_2 and u_3 components of the elastic wavefield, respectively, obtained using our third-order HMsFEM, and Figs. 10c, d and e show the amplitude differences between the HMsFEM coarse-mesh solution and the conventional SEM fine-mesh solution, respectively. The relative errors associated with our second-order HMsFEM solution is merely 15.5 percent, while that associated with the third-order HMsFEM is only 5.7 percent. In contrast, the relative errors associated with the second- and third-order conventional SEM on the 20 m coarse mesh are 32.3 percent and 26.1 percent, respectively. Evidently, our HMsFEM is more accurate than the conventional SEM on the coarse mesh. The CPU time associated with our second- and third-order HMsFEM are approximately 56 s and 359 s, respectively. In the 3D case, the computations of multiscale basis functions for the third-order HMsFEM is long (3,874 s), which makes the advantage of our HMsFEM less significant compared with the conventional SEM. Again, we remark that the computational costs associated with the multiscale basis functions for a fixed model is a one-time computation before the actual wavefield propagation starts. Therefore, with appropriate parallel computing strategies, the computation of multiscale basis functions can be easily accelerated, making our HMsFEM an efficient tool for elastic wave modeling. We provides the details of the tests and compare the efficiency between the conventional SEM and our HMsFEM in Table 2. The comparison resembles that for the aforementioned 2D random fracture model, manifesting that our HMsFEM is more accurate and computationally efficient than, or at least a good alternative to, the conventional SEM for simulating elastic wavefield propagation in strongly heterogeneous media.

Figure 8: The reference wavefields at $t=1$ s computed using the conventional SEM on the fine mesh. The panel in (a) is the u_1 component, (b) is the u_2 component while (c) is the u_3 component. The CPU time to obtain these fine-mesh SEM solutions is approximately 3022 s.

Figure 9: The (a) u_1, (b) u_2 and (c) u_3 components of the elastic wavefield solution obtained using our second-order HMsFEM on the coarse mesh. The differences between the coarse-mesh HMsFEM solutions and the fine-mesh SEM solutions are shown in (d), (e) and (f) for the u_1, u_2 and u_3 components, respectively. The CPU time to obtain the coarse-mesh HMsFEM solutions is approximately 56 s.

Figure 10: The (a) u_1, (b) u_2 and (c) u_3 components of the elastic wavefield solution obtained using our third-order HMsFEM on the coarse mesh. The differences between the coarse-mesh HMsFEM solutions and the fine-mesh SEM solutions are shown in (d), (e) and (f) for the u_1, u_2 and u_3 components, respectively. The CPU time to obtain the coarse-mesh HMsFEM solutions is approximately 359 s.

Method	m	N	r	T_{offline} (s)	T_{online} (s)	ε
SEM	2	100	1	780.9	3021.7	/
SEM	1	100	1	80.6	259.5	0.189
SEM	2	20	5	55.7	55.4	0.323
SEM	3	20	5	365.2	365.2	0.261
HMsFEM	2	20	5	311.4	55.7	0.155
HMsFEM	3	20	5	3873.6	358.8	0.057

Table 2: Parameter settings, computational time consumption and relative errors of the simulation results for the 3D random fracture model. The meanings of these parameters can be found in Table. 1.

4 Conclusions

We have developed a novel high-order multiscale finite-element method for elastic wavefield modeling in strongly heterogeneous media in the time domain. We construct high-order multiscale basis functions from two types of local-domain problems. We further obtain construct the final multiscale basis functions based on the cardinal interpolation property of these solved bases and a linear combination. These multiscale basis functions are medium dependent and therefore can effectively convey the fine-scale medium information to the coarse mesh to ensure high-order accuracy of elastic wave modeling. These basis functions lead to significantly reduced system matrices compared with the conventional spectral-element method. We have used one 2D numerical example and one 3D numerical example to demonstrate the computational efficiency of our high-order multiscale finite-element method, and have found that our new method is more efficient than the conventional spectral-element method in modeling elastic wave propagation in strongly heterogeneous media. Our future work will focus on developing appropriate strategy to improve the efficiency of high-order multiscale basis function computation.

Acknowledgment

Eric Chung's research is partially supported by Hong Kong RGC General Research Fund (Project 14304217) and CUHK Direct Grant for Research 2017-18.

References

[1] Patrick R. Amestoy, Iain S. Duff, Jean-Yves L'Excellent, and François-Henry Rouet. Parallel computation of entries of A^{-1}. *SIAM Journal on Scientific Computing*, 37(2):C268–C284, 2015.

[2] José M. Carcione. *Wave Fields in Real Media: Wave Propagation in Anisotropic, Anelastic, Porous and Electromagnetic Media (Third Edition)*. Elsevier, Amsterdam,

Netherlands, 2015.

[3] Olivier Cessenat and Bruno Després. Using plane waves as base functions for solving time harmonic equations with the ultra weak variational formulation. *Journal of Computational Acoustics*, 11(02):227–238, 2003.

[4] Eric T Chung, Yalchin Efendiev, and Richard L Gibson Jr. An energy-conserving discontinuous multiscale finite element method for the wave equation in heterogeneous media. *Advances in Adaptive Data Analysis*, 3(01n02):251–268, 2011.

[5] Eric T. Chung, Yalchin Efendiev, and Wing Tat Leung. Generalized multiscale finite element methods for wave propagation in heterogeneous media. *Multiscale Modeling & Simulation*, 12(4):1691–1721, 2014.

[6] Eric T. Chung, Chi Yeung Lam, and Jianliang Qian. A staggered discontinuous Galerkin method for the simulation of seismic waves with surface topography. *Geophysics*, 80(4):T119–T135, 2015.

[7] Eric T. Chung, Chi Yeung Lam, and Jianliang Qian. A staggered discontinuous Galerkin method for the simulation of seismic waves with surface topography. *Geophysics*, 80(4):T119–T135, 2015.

[8] Eric T. Chung and Tang Fei Yu. Staggered-grid spectral element methods for elastic wave simulations. *Journal of Computational and Applied Mathematics*, 285(0):132 – 150, 2015.

[9] Gary Cohen and Sandrine Fauqueux. Mixed finite elements with mass-lumping for the transient wave equation. *Journal of Computational Acoustics*, 8 (1):171–188, 2000.

[10] Régis Cottereau and Ruben Sevilla. Stability of an explicit high-order spectral element method for acoustics in heterogeneous media based on local element stability criteria. *International Journal for Numerical Methods in Engineering*, 116(4):223–245, 2018.

[11] Jonás D. De Basabe, Mrinal K. Sen, and Mary F. Wheeler. The interior penalty discontinuous Galerkin method for elastic wave propagation: grid dispersion. *Geophysical Journal International*, 175(1):83–93, 2008.

[12] Y. Efendiev, T. Y. Hou, and V. Ginting. Multiscale finite element methods for nonlinear problems and their applications. *Commun. Math. Sci.*, 2(4):553–589, 12 2004.

[13] Yalchin Efendiev, Juan Galvis, and Thomas Y. Hou. Generalized Multiscale Finite Element Methods (GMsFEM). *Journal of Computational Physics*, 251:116–135, October 2013.

[14] Abdellah El Kacimi and Omar Laghrouche. Numerical modelling of elastic wave scattering in frequency domain by the partition of unity finite element method. *International journal for numerical methods in engineering*, 77(12):1646–1669, 2009.

[15] Björn Engquist and Lexing Ying. Sweeping preconditioner for the helmholtz equation: Moving Perfectly Matched Layers. *Multiscale Modeling & Simulation*, 9(2):686–710, 2011.

[16] Charbel Farhat, Isaac Harari, and Ulrich Hetmaniuk. A discontinuous galerkin method with lagrange multipliers for the solution of helmholtz problems in the mid-frequency regime. *Computer Methods in Applied Mechanics and Engineering*, 192(11):1389 – 1419, 2003.

[17] Andreas Fichtner. *Full Seismic Waveform Modelling and Inversion*. Springer, Berlin, 2011.

[18] Bengt Fornberg. The pseudospectral method: Accurate representation of interfaces in elastic wave calculations. *Geophyscis*, 53(5):625–637, 1988.

[19] Shubin Fu, Yalchin Efendiev, Kai Gao, and Richard L. Gibson Jr. Multiscale modeling of acoustic wave propagation in 2D heterogeneous media using local spectral basis functions. *SEG Technical Program Expanded Abstracts 2013*, pages 3553–3558, 2013.

[20] Shubin Fu and Kai Gao. A fast solver for the helmholtz equation based on the generalized multiscale finite-element method. *Geophysical Journal International*, 211(2):819–835, 2017.

[21] Kai Gao, Eric T. Chung, Richard L. Gibson, Shubin Fu, and Yalchin Efendiev. A numerical homogenization method for heterogeneous, anisotropic elastic media based on multiscale theory. *Geophysics*, 80(4):D385–D401, 2015.

[22] Kai Gao, Shubin Fu, and Eric T. Chung. An efficient multiscale finiteâ€ • element method for frequencyâ€ • domain seismic wave propagation. *Bulletin of the Seismological Society of America*, 108(2):966, 2018.

[23] Kai Gao, Shubin Fu, and Eric T. Chung. An efficient multiscale finiteâ€ • element method for frequencyâ€ • domain seismic wave propagationan. *Bulletin of the Seismological Society of America*, 108(2):966, 2018.

[24] Kai Gao and Lianjie Huang. An improved rotated staggered-grid finite-difference method with fourth-order temporal accuracy for elastic-wave modeling in anisotropic media.

Journal of Computational Physics, 350:361 – 386, 2017.

[25] Richard L. Gibson, Kai Gao, Eric Chung, and Yalchin Efendiev. Multiscale modeling of acoustic wave propagation in 2D media. *Geophysics*, 79(2):T61, 2014.

[26] J. Gozani, A. Nachshon, and E. Turkel. Conjugate gradient coupled with multigrid for an indefinite problem. *Advances in Computer Methods for Partial Differential Equations V*, pages 425–427, 1984.

[27] R. Hiptmair, A. Moiola, and I. Perugia. Plane wave discontinuous Galerkin methods for the 2d Helmholtz equation: Analysis of the p-version. *SIAM Journal on Numerical Analysis*, 49(1):264–284, 2011.

[28] Lise-Marie Imbert-Gérard and Bruno Després. A generalized plane-wave numerical method for smooth nonconstant coefficients. *IMA Journal of Numerical Analysis*, 34(3):1072–1103, 2014.

[29] Martin Käser and Michael Dumbser. An arbitrary high-order discontinuous Galerkin method for elastic waves on unstructured meshes – I. The two-dimensional isotropic case with external source terms. *Geophysical Journal International*, 166(2):855–877, 2006.

[30] Marek Klimczak and Witold Cecot. An adaptive msfem for nonperiodic viscoelastic composites. *International Journal for Numerical Methods in Engineering*, 114(8):861–881, 2018.

[31] Dimitri Komatitsch and Jeroen Tromp. Introduction to the spectral element method for three-dimensional seismic wave propagation. *Geophysical Journal International*, 139(3):806–822, 1999.

[32] Dimitri Komatitsch and Jean-Pierre Vilotte. The spectral element method: An efficient tool to simulate the seismic response of 2d and 3d geological structures. *Bulletin of the Seismological Society of America*, 88(2):368–392, 1998.

[33] Pawel Kudela. Parallel implementation of spectral element method for lamb wave propagation modeling. *International Journal for Numerical Methods in Engineering*, 106(6):413–429, 2016.

[34] Alan R. Levander. Fourth-order finite-difference P-SV seismograms. *Geophysics*, 53(11):1425–1436, 1988.

[35] Vadim Lisitsa and Dmitriy Vishnevskiy. Lebedev scheme for the numerical simulation of wave propagation in 3D anisotropic elasticityâ€¡. *Geophysical Prospecting*,

58(4):619–635, 2010.

[36] Yang Liu. Optimal staggered-grid finite-difference schemes based on least-squares for wave equation modelling. *Geophysical Journal International*, 197:1033–1047, 2014.

[37] René Matzen. An efficient finite element time-domain formulation for the elastic second-order wave equation: A non-split complex frequency shifted convolutional pml. *International Journal for Numerical Methods in Engineering*, 88(10):951–973, 2011.

[38] J. M. Melenk and S. Sauter. Convergence analysis for finite element discretizations of the Helmholtz equation with Dirichlet-to-Neumann boundary conditions. *Mathematics of Computation*, 79(272):1871–1914, 2010.

[39] Peter Moczo, Jozef Kristek, Martin Galis, Emmanuel Chaljub, and Vincent Etienne. 3-D finite-difference, finite-element, discontinuous-Galerkin and spectral-element schemes analysed for their accuracy with respect to P-wave to S-wave speed ratio. *Geophysical Journal International*, 187(3):1645–1667, 2011.

[40] Peter Moczo, Johan O.A. Robertsson, and Leo Eisner. The finite-difference time-domain method for modeling of seismic wave propagation. In Valerie Maupin Ru-Shan Wu and Renata Dmowska, editors, *Advances in Wave Propagation in Heterogenous Earth*, volume 48 of *Advances in Geophysics*, pages 421 – 516. Elsevier, 2007.

[41] Luke N. Olson and Jacob B. Schroder. Smoothed aggregation for Helmholtz problems. *Numerical Linear Algebra with Applications*, 17(2-3):361–386, 2010.

[42] Jie Peng, Junxian Wang, and Shi Shu. Adaptive bddc algorithms for the system arising from plane wave discretization of helmholtz equations. *International Journal for Numerical Methods in Engineering*, 2018.

[43] Jack Poulson, Björn Engquist, Siwei Li, and Lexing Ying. A parallel sweeping preconditioner for heterogeneous 3d Helmholtz equations. *SIAM Journal on Scientific Computing*, 35(3):C194–C212, 2013.

[44] Erik H. Saenger, Norbert Gold, and Serge A. Shapiro. Modeling the propagation of elastic waves using a modified finite-difference grid. *Wave Motion*, 31(1):77 – 92, 2000.

[45] Arkaprabha Sengupta, Panayiotis Papadopoulos, and Robert L Taylor. A multiscale finite element method for modeling fully coupled thermomechanical problems in solids. *International Journal for Numerical Methods in Engineering*, 91(13):1386–1405, 2012.

[46] Linlin Shi, Yuanguo Zhou, Jia-Min Wang, Mingwei Zhuang, Na Liu, and Qing Huo Liu.

Spectral element method for elastic and acoustic waves in frequency domain. *Journal of Computational Physics*, 327:19 – 38, 2016.

[47] Christiaan C. Stolk. A rapidly converging domain decomposition method for the Helmholtz equation. *Journal of Computational Physics*, 241:240 – 252, 2013.

[48] Godehard Sutmann. Compact finite difference schemes of sixth order for the Helmholtz equation. *Journal of Computational and Applied Mathematics*, 203(1):15 – 31, 2007.

[49] Lonny L. Thompson and Peter M. Pinsky. A Galerkin least-squares finite element method for the two-dimensional Helmholtz equation. *International Journal for Numerical Methods in Engineering*, 38(3):371–397, 1995.

[50] Paul Tsuji, Jack Poulson, Björn Engquist, and Lexing Ying. Sweeping preconditioners for elastic wave propagation with spectral element methods. *ESAIM: Mathematical Modelling and Numerical Analysis*, 48(2):433–447, 2014.

[51] Eli Turkel, Charbel Farhat, and Ulrich Hetmaniuk. Improved accuracy for the helmholtz equation in unbounded domains. *International Journal for Numerical Methods in Engineering*, 59(15):1963–1988, 2004.

[52] Eli Turkel, Dan Gordon, Rachel Gordon, and Semyon Tsynkov. Compact 2d and 3d sixth order schemes for the helmholtz equation with variable wave number. *Journal of Computational Physics*, 232(1):272 – 287, 2013.

[53] Jean Virieux. P-SV wave propagation in heterogeneous media: Velocity-stress finite-difference method. *Geophysics*, 51(4):889–901, 1986.

[54] Lucas C. Wilcox, Georg Stadler, Carsten Burstedde, and Omar Ghattas. A high-order discontinuous Galerkin method for wave propagation through coupled elastic-acoustic media. *Journal of Computational Physics*, 229(24):9373 – 9396, 2010.

[55] Dinghui Yang, Jiwen Teng, Zhongjie Zhang, and Enru Liu. A nearly analytic discrete method for acoustic and elastic wave equations in anisotropic media. *Bulletin of the Seismological Society of America*, 93(2):882–890, 2003.

[56] Qiwei Zhan, Qiang Ren, Mingwei Zhuang, Qingtao Sun, and Qing Huo Liu. An exact riemann solver for wave propagation in arbitrary anisotropic elastic media with fluid coupling. *Computer Methods in Applied Mechanics and Engineering*, 329:24 – 39, 2018.

[57] Lingxue Zhu and Haijun Wu. Preasymptotic error analysis of CIP-FEM and FEM for Helmholtz equation with high wave number. Part II: hp version. *SIAM Journal on*

Numerical Analysis, 51(3):1828–1852, 2013.

Highlights:

- We develop a higher multiscale finite element method for elastic wave propagation in strongly heterogeneous media ;
- This new approach is very accurate and efficient due to the higher oder basis functions are used.
- The idea of constructing higher oder multiscale basis functions can be extended to other Galerkin formulations.